N90-27997

von Karman Institute for Fluid Dynamics

Lecture Series 1990-03

COMPUTATIONAL FLUID DYNAMICS

March 5–9, 1990

TAILORING EXPLICIT-MARCHING SCHEMES
TO IMPROVE CONVERGENCE CHARACTERISTICS

K.G. Powell & B. van Leer

U. Michigan, USA

Tailoring Explicit Time-Marching Schemes to Improve Convergence Characteristics

Kenneth G. Powell and Bram van Leer
Department of Aerospace Engineering
The University of Michigan
Ann Arbor, MI USA

March 1990

1 Abstract

Multi-stage time-stepping schemes that are tailored to chosen spatial-differencing operators are derived and tested. The schemes are constructed to give optimal damping of the high-frequency waves, making them ideal for use with multi-grid acceleration. The concept of characteristic time-stepping, necessary for the extension of the scalar analysis to systems of equations, is presented. The schemes show a marked improvement over Runge-Kutta schemes.

2 Introduction

Numerical methods for the computation of steady flows can be divided into two classes: explicit and implicit methods. Implicit methods have been favored for steady-state calculations for a long time; this relates to the elliptic nature of the equations of steady subsonic flow. Representative of the class of implicit methods used for solving the steady Euler and Navier-Stokes equations are the Approximate-Factorization methods developed at NASA Ames Research Center [1] during the seventies. The strongest argument in favor of implicit methods is the relatively large reduction in residual that can be achieved in one iteration step. This is due in part to the numerical coupling of computational cells from one boundary to another in a single iteration.

Explicit techniques require many more iterations than implicit techniques, but each iteration is relatively cheap. The numerical coupling from boundary to boundary can be achieved at low computational cost by the use of coarse-grid information, in a so-called multi-grid strategy. Once multi-grid relaxation has been successfully implemented, explicit methods have only advantages over implicit methods. They require little storage, are easily implemented on vector and parallel architectures, and naturally allow local grid refinements [2]. The latter advantage is crucial, since adaptive grid refinement seems to be the most promising way to efficiently obtain spatial accuracy in complex problems. The most popular explicit

methods for computing steady solutions of the Euler and Navier-Stokes equations are the multi-stage methods pioneered by Jameson *et al* [3].

This lecture concerns the design of explicit multi-stage schemes for the Euler equations, for use in a multi-grid strategy. The requirements for single-grid and multi-grid schemes differ somewhat, although probably not as much as has been traditionally assumed. For single-grid computations the standard approach is always to take the maximum time-step allowed by the scheme's stability condition, the underlying idea being that the asymptotic steady state will then be reached in fewer steps. This is not necessarily the best strategy for multi-grid computations.

In a multi-grid procedure, one special task of the marching scheme is to remove high-frequency components of the error while marching; the multi-grid strategy acts to remove low-frequency components through the use of coarse-grid representations of the solution [4]. In all marching schemes presently in use, the best damping properties are achieved for a time-step that is substantially less than the maximum allowed by stability considerations.

To make a marching scheme a good multi-grid "smoother," the temporal and spatial discretization must be matched to each other. Since the spatial discretization dictates the final accuracy of the solution, the most natural way is to select a spatial discretization and design the time discretization in such a way that short waves are effectively damped. In the multi-grid code developed by Jameson [5], this is achieved by appropriately choosing the values of the parameters of a multi-stage integration method. The analysis on which the choice of parameters is based is strictly scalar and one-dimensional, and is carried out by trial and error. The material presented in this lecture suggests that a more thorough and comprehensive analysis of the damping properties of multi-stage schemes, and its proper extension to systems of multi-dimensional equations, can significantly improve the performance of the multi-grid procedure.

The core of this presentation is the analysis and optimization of the damping properties of multi-stage schemes for the one-dimensional linear convection equation (Section 2); the results can be applied to a nonlinear convection equation (Section 3), owing to the well-known scalar preconditioning technique of using "local" time steps. The extension to the system of the one-dimensonal Euler equations requires the use of "characteristic" time-steps, equivalent to preconditioning by a matrix (Section 4). The successful application to multi-dimensional scalar equations depends on the availability of a technique to damp numerical signals that move normal to the physical transport directions; application to the multidimensional Euler equations in addition requires a new matrix preconditioning. These two techniques are still in development (Section 5).

The analysis is illustrated with numerical experiments throughout Sections 3, 4 and 5 In Section 6 the results are summarized and a prognosis is given for explicit multi-grid relaxation for the multi-dimensional Euler equations.

3 The Multi-Stage Scheme as a High-Frequency Filter

The generic marching scheme used is a *two-stage* or *predictor-corrector* integration method for the linear ordinary differential equation

$$\frac{du}{dt} = \lambda u, \qquad \lambda \in C \ , \tag{1}$$

that is,

$$\tilde{u} = u^n + \alpha \Delta t \lambda u^n \tag{2a}$$

$$u^{n+1} = u^n + \Delta t \lambda \tilde{u} \tag{2b}$$

$$= \left[1 + \lambda \Delta t + \alpha \left(\lambda \Delta t \right)^2 \right] u^n. \tag{2c}$$

Here α is the *time-step ratio* and is a free parameter. As seen from Equation 2c, the stability and damping properties of the scheme are associated with the complex polynomial

$$P_2(z, \alpha) = 1 + z + \alpha z^2, \qquad z \equiv \lambda \Delta t. \tag{3a}$$

This polynomial has two complex-conjugate roots, $z_1(\alpha)$ and $z_2(\alpha) = z_1^*(\alpha)$, with

$$z_1(\alpha) = -\frac{1}{2\alpha} - \frac{i}{2\alpha}\sqrt{4\alpha - 1}; \tag{3b}$$

these may be moved along the circle

$$\left[\Re(z_0) + 1 \right]^2 + \left[\Im(z_0) \right]^2 = 1 \tag{3c}$$

by varying α.

When a *partial* differential equation is interpreted by the method of lines, λ represents the Fourier transform of the spatial differencing operator, and depends on the spatial frequency ξ or, more specifically, on the spatial wave number

$$\beta = 2\pi\xi\Delta x. \tag{4}$$

For instance, when solving the convection equation

$$\frac{\partial u}{\partial t} = -c\frac{\partial u}{\partial x}, \qquad c > 0, \tag{5}$$

use of upwind differencing for the spatial derivative gives

$$\Delta t \frac{\partial u}{\partial t} = -\nu \left[u(x,t) - u(x - \Delta x, t) \right], \tag{6}$$

where the non-dimensional time step,

$$\nu = \frac{c\Delta t}{\Delta x}, \tag{7}$$

is the Courant-Friedrichs-Lewy (CFL) number. After inserting harmonic data

$$u(x) = u_0 e^{2\pi i \xi x}, \tag{8}$$

Equation 6 reduces to Equation 1 with

$$\lambda \Delta t \equiv z(\beta, \nu) = -\nu \left(1 - e^{-i\beta}\right). \tag{9}$$

The key observation to be made here is that, *for any β_0 in the high-frequency range* $[\pi/2, \pi]$, *it is possible to make $z(\beta_0, \nu) \equiv \lambda(\beta_0)\Delta t$ coincide with a zero of $P_2(z, \alpha)$, by choosing a particular combination of α and Δt*. This results in perfect damping of the wave with wave number β_0 in one application of the predictor-corrector scheme. Using strings of predictor-corrector schemes, tuned to damp different frequencies, the entire high-frequency range can be damped to arbitrarily low levels.

Strings of predictor-corrector methods generate multi-stage methods with an even number of stages; to get an odd number of stages, a single application of the "forward-Euler" scheme

$$u^{n+1} = u^n + \Delta t \lambda u^n \tag{10a}$$

$$= (1 + \lambda \Delta t) u^n, \tag{10b}$$

should be included in the string. The forward-Euler step has amplification factor

$$P_1(z) = 1 + z; \tag{11}$$

this polynomial has one zero, at

$$z_1 = -1. \tag{12}$$

A second key observation is that, *for any fixed number of stages, there is an optimum scheme, in the L_∞ sense, reducing all of the high frequencies to an amplitude not exceeding a unique minimal threshold level*. It is these "optimally smoothing" multi-stage schemes that are developed here, for use in multi-grid Euler codes.

3.1 Optimal Multi-Stage Schemes for General Spatial Differencing

For a general spatial-differencing operator, whether convective or diffusive, or a combination of both, the Fourier transform can still be written as

$$\lambda \Delta t \equiv z(\beta, \nu) = \nu[a(\beta) + ib(\beta)], \tag{13}$$

where ν is a nondimensional time-step; keeping to the framework of convective equations for the sake of example, ν shall continue to be referred to as the CFL number. For a frequency β_0 to be perfectly damped by the two-stage scheme, associated with the polynomial 3a, it is necessary to set $z_1(\alpha) = z(\beta_0, \nu)$, or

$$-\frac{1}{2\alpha} - \frac{i}{2\alpha}\sqrt{4\alpha - 1} = \nu[a(\beta_0) + ib(\beta_0))], \tag{14}$$

4

with solution

$$\alpha_0 \;=\; \frac{a_0^2 + b_0^2}{4a_0^2}, \tag{15a}$$

$$\nu_0 \;=\; \frac{2|a_0|}{a_0^2 + b_0^2}, \tag{15b}$$

where $a_0 \equiv a(\beta_0)$, $b_0 \equiv b(\beta_0)$. The single-step forward-Euler scheme can only damp the frequency for which the Fourier transform (Equation 13) is real-valued; for any finite-difference operator this means

$$\beta_0 = \pi : \tag{16}$$

the corresponding CFL number is

$$\nu_0 = \frac{1}{|a_0|}. \tag{17}$$

For the first-order upwind differencing operator, the optimization of the high-frequency damping in a string of predictor-corrector and single-step operators can be done analytically [6]; for more complex differencing operators this is no longer feasible. An iterative method for solving this minimax problem is described below.

Suppose that, in optimizing an m–stage method (m even or odd), as an initial guess or from the previous iteration, a set of perfectly damped frequencies β_k, $k = 1,\ldots,\hat{m}$, with $\hat{m} = \text{int}(m/2)$, has been obtained; let these be represented by the vector β_0. There are $\hat{m} + 1$ local maxima of $|P_m(\beta)|$ on the interval $[\pi/2, \pi]$, called M_k, $k = 1,\ldots,\hat{m} + 1$; these can be found by a numerical search. As long as these values are not equal, the scheme is not optimal. The lack of equality is expressed in the form of an L_2-residual

$$R_0 \equiv R(\beta_0) = \sum_{k=1}^{\hat{m}} (M_{k+1}(\beta_0) - M_k(\beta_0))^2, \tag{18}$$

which is then brought closer to zero by one step of a Newton process. Since $\hat{m}$ frequencies must be updated, $\hat{m}$ independent residual values must be obtained. For this purpose, all frequencies β_k are perturbed by a small amount $\delta\beta$, i.e.,

$$\beta_k' = \beta_k + \delta\beta, \tag{19}$$

and $\hat{m}$ new frequency vectors $\beta^{(i)}$ are formed such that the first i frequencies are perturbed, i.e.:

$$\beta^{(i)} = (\beta_1',\ldots,\beta_i',\beta_{i+1},\ldots,\beta_{\hat{m}}), \qquad i = 1,\ldots,\hat{m}. \tag{20}$$

For all of these frequency vectors, residuals are obtained in the manner described above; these are called $R^{(i)}$,

$$R^{(i)} \equiv R(\beta^{(i)}), \quad i = 1,\ldots,\hat{m}, \tag{21}$$

and are collectively indicated by the residual vector R:

$$R \equiv (R^{(1)},\ldots,R^{(\hat{m})}). \tag{22}$$

The Jacobian matrix $J \equiv dR(\beta)/d\beta$ of the residual vector with respect to the frequency vector, needed for a Newton step, is computed approximately by means of finite-differencing.

5

Defining the vectors $\boldsymbol{\beta}^{(i,j)}$ as $\boldsymbol{\beta}^{(i)}$ with the jth component either perturbed or 'unperturbed', i.e.

$$\boldsymbol{\beta}^{(i,j)} = (\beta'_1, \ldots, \beta'_{j-1}, \beta_j, \beta'_{j+1}, \ldots, \beta'_i, \beta_{i+1}, \ldots, \beta_{\hat{m}}), \qquad j \leq i, \qquad (23a)$$

$$\boldsymbol{\beta}^{(i,j)} = (\beta'_1, \ldots, \beta'_i, \beta_{i+1}, \ldots, \beta_{j-1}, \beta'_j, \beta_{j+1}, \ldots, \beta_{\hat{m}}), \qquad j > i, \qquad (23b)$$

and defining the corresdponding residuals $R^{(i,j)}$,

$$R^{(i,j)} \equiv R\left(\boldsymbol{\beta}^{(i,j)}\right), \qquad (24)$$

some of which have been calculated previously; the elements of the Jacobian are then evaluated according to

$$J_{k\ell} = \frac{\partial R^{(k)}}{\partial \beta_\ell} \qquad (25a)$$

$$= \frac{R^{(k)} - R^{(k,\ell)}}{\delta\beta}, \qquad \ell \leq k; \qquad (25b)$$

$$J_{k\ell} = \frac{R^{(k,\ell)} - R^{(k)}}{\delta\beta}, \qquad \ell > k. \qquad (25c)$$

The Newton step amounts to solving for the correction vector $\Delta\boldsymbol{\beta}$ from

$$-\mathbf{J}\Delta\boldsymbol{\beta} = \mathbf{R}, \qquad (26)$$

and updating $\boldsymbol{\beta}_0$:

$$\boldsymbol{\beta}_o := \boldsymbol{\beta}_o + \Delta\boldsymbol{\beta}. \qquad (27)$$

The above procedure was implemented to find the first six multi-stage schemes with optimal high-frequency damping for the spatial differencing operator with Fourier transform

$$\lambda\Delta t = -\nu(1 - \exp^{-i\beta})\left\{1 + \frac{1-\kappa}{4}(1 - \exp^{-i\beta}) + \frac{1+\kappa}{4}(\exp^{i\beta} -1)\right\}, \qquad (28)$$

corresponding to higher-order upwind-biased differencing [7]. The parameter κ regulates the upwind bias: $\kappa = 1$ yields central differencing, $\kappa = -1$ second-order-accurate fully upwind differencing, $\kappa = 1/3$ third-order-accurate upwind-biased differencing. For this latter choice, the damping properties of the six schemes are displayed in Figures 1 to 11.

The important parameters of the first six multi-stage schemes for several spatial-differencing operators are listed in Tables 1-5; these require some explanation. Specifically, the quantities α_k listed in Tables 1-3 are not the time-step ratios of the constituent predictor-corrector schemes, but the time-step ratios arising in the *practical* implementation of an m-stage scheme, i.e.,

$$u^{(0)} = u^n, \qquad (29a)$$

$$u^{(k)} = u^{(0)} + \alpha_k \Delta t\, \lambda u^{(k-1)}, \qquad k = 1, \ldots, m, \qquad (29b)$$

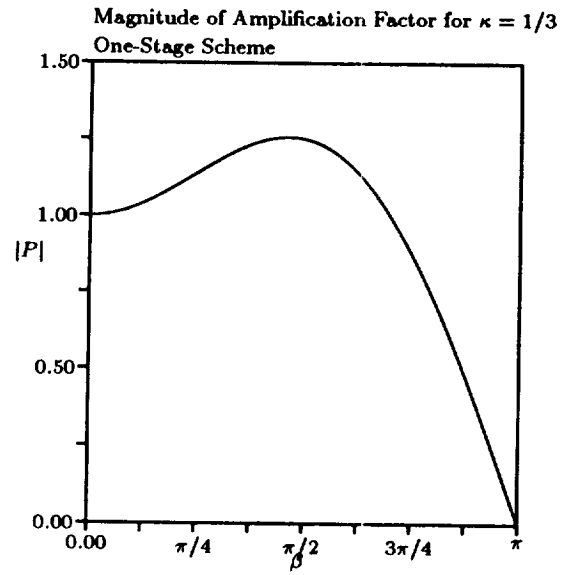$$u^{n+1} = u^{(m)}. \qquad (29c)$$

6

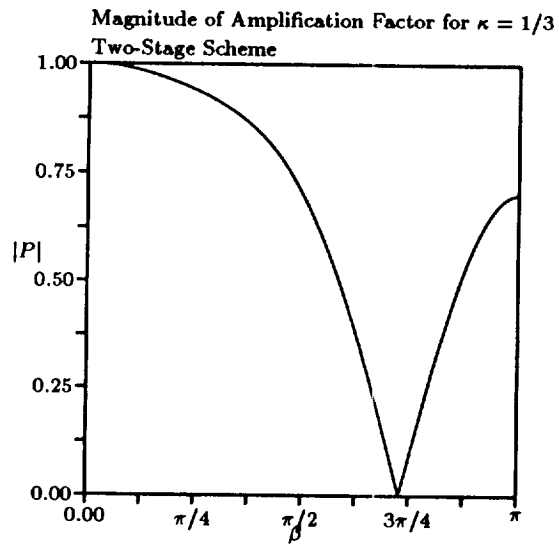Figure 1: Amplification factor; third-order, one-stage scheme

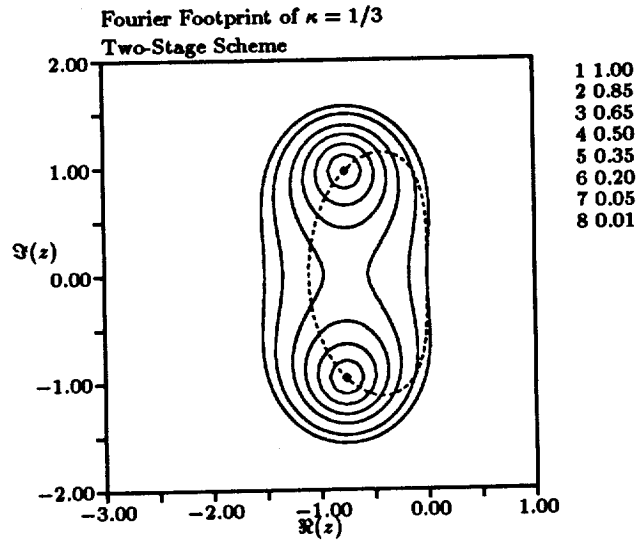Figure 2: Amplification factor; third-order, two-stage scheme

7

Fourier Footprint of $\kappa = 1/3$ Two-Stage Scheme

1	1.00
2	0.85
3	0.65
4	0.50
5	0.35
6	0.20
7	0.05
8	0.01

Figure 3: Locus and contours; third-order, two-stage scheme

Magnitude of Amplification Factor for $\kappa = 1/3$ Three-Stage Scheme
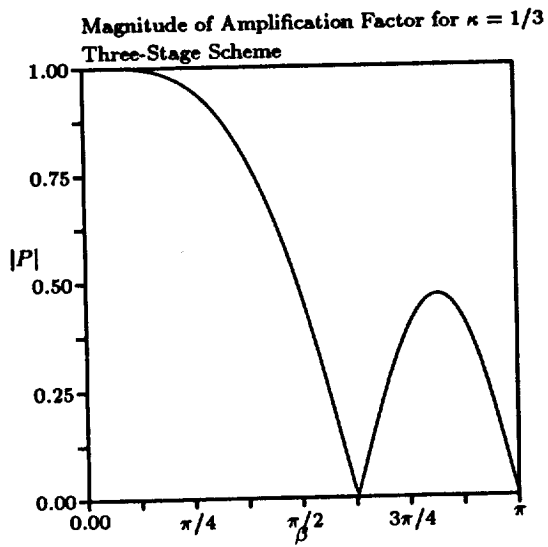
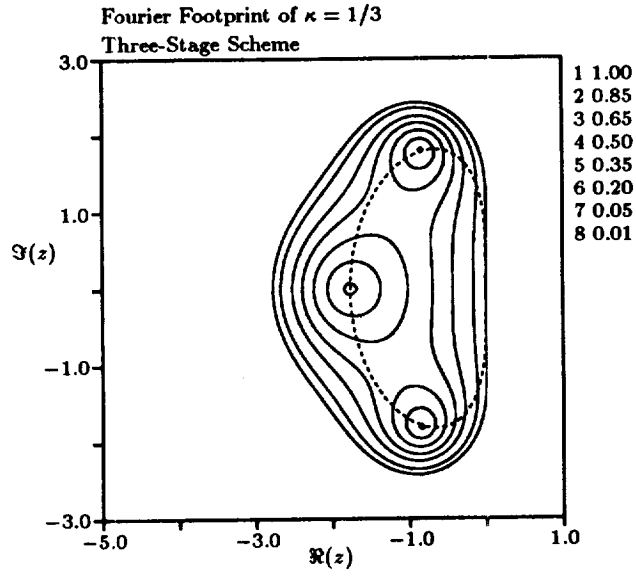Figure 4: Amplification factor; third-order, three-stage scheme

8

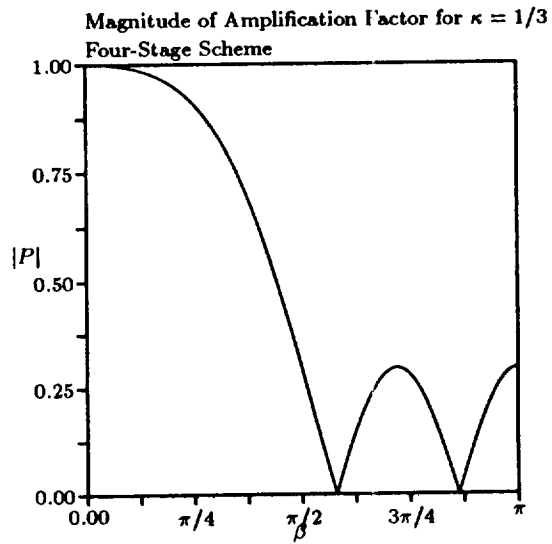Figure 5: Locus and contours; third-order, three-stage scheme

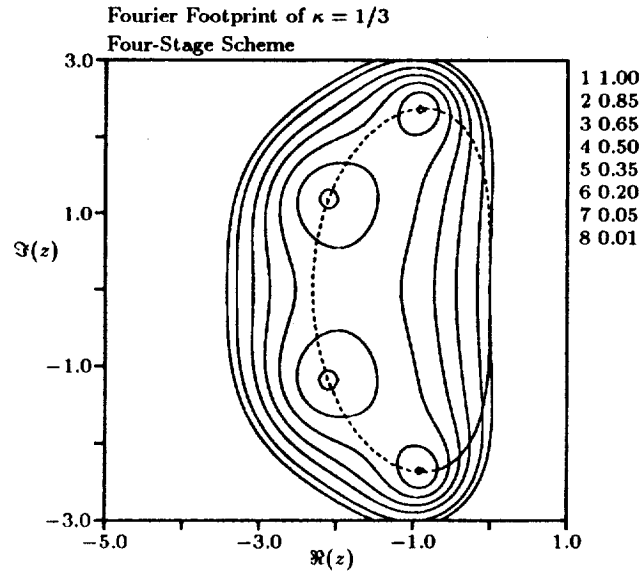Figure 6: Amplification factor; third-order, four-stage scheme

9

Fourier Footprint of $\kappa = 1/3$
Four-Stage Scheme

1	1.00
2	0.85
3	0.65
4	0.50
5	0.35
6	0.20
7	0.05
8	0.01

Figure 7: Locus and contours; third-order, four-stage scheme

Magnitude of Amplification Factor for $\kappa = 1/3$
Five-Stage Scheme

Figure 8: Amplification factor; third-order, five-stage scheme

10

Fourier Footprint of $\kappa = 1/3$
Five-Stage Scheme

1	1.00
2	0.85
3	0.65
4	0.50
5	0.35
6	0.20
7	0.05
8	0.01
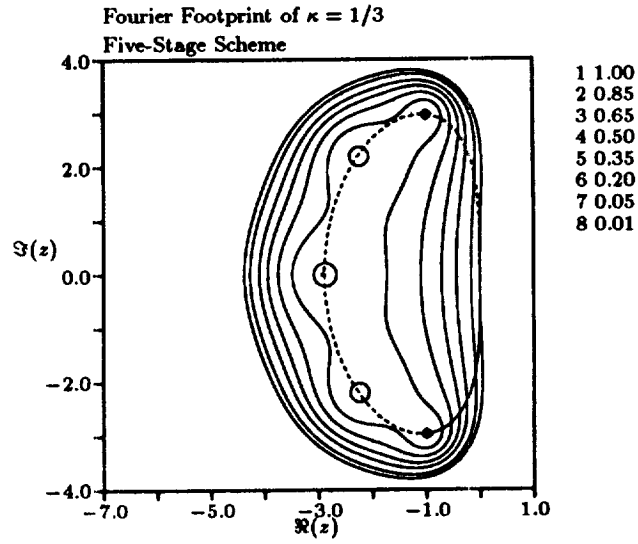
Figure 9: Locus and contours; third-order, five-stage scheme

Magnitude of Amplification Factor for $\kappa = 1/3$
Six-Stage Scheme

Figure 10: Amplification factor; third-order, six-stage scheme

11

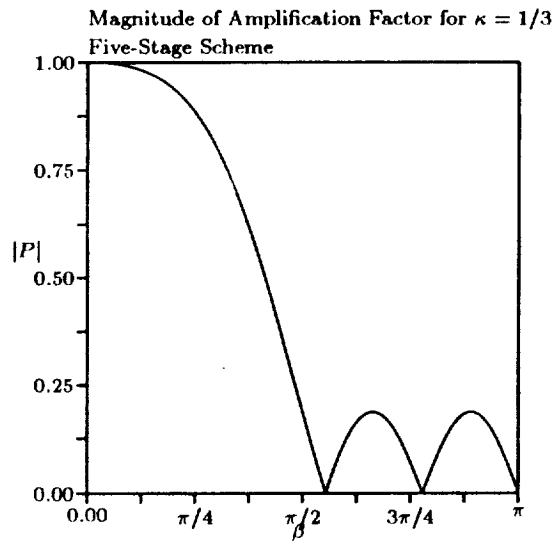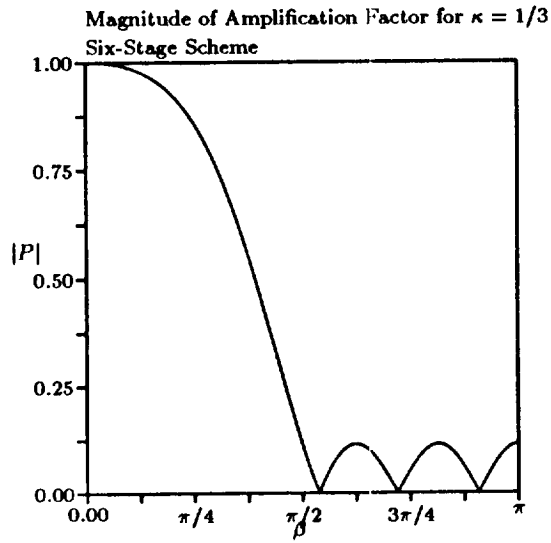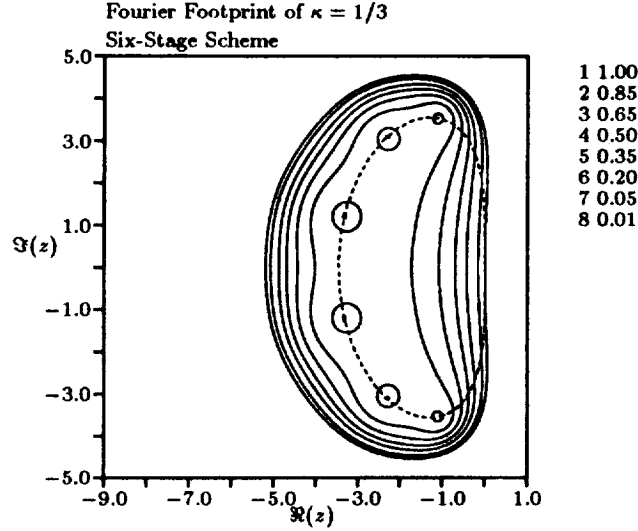Figure 11: Locus and contours; third-order, six-stage scheme

Note that the mth step always spans the full time-interval Δt, so that

$$\alpha_m = 1. \tag{30}$$

The amplification factor of the above scheme can be written as

$$P_m(z) = 1 + z(1 + \alpha_{m-1}z(1 + \alpha_{m-2}z(\ldots\ldots(1 + \alpha_2 z(1 + \alpha_1 z))\ldots))), \tag{31a}$$

where z now corresponds to the CFL number for the full time-interval. The coefficients α_k thus are found by multiplying out the string of polynomials of the form 3a and 11, and re-scaling z such that the linear term gets a coefficient of unity.

For example, the three-stage first-order method, regarded as a string of a single step and a predictor-corrector operator, can be shown to have the amplification factor

$$P_3(z) = (1 + \frac{z}{2})(1 + z + \frac{2}{5}z^2), \tag{32}$$

with z corresponding to a CFL number of 1; it can be rewritten as

$$P_3(z) = 1 + \frac{3}{2}z + \frac{9}{10}z^2 + \frac{1}{5}z^3 \tag{33}$$

$$= 1 + \left(\frac{3}{2}z\right) + \frac{2}{5}\left(\frac{3}{2}z\right)^2 + \frac{8}{135}\left(\frac{3}{2}z\right)^3 \tag{34}$$

or

$$P_3(\bar{z}) = 1 + \bar{z} + \frac{2}{5}\bar{z}^2 + \frac{8}{135}\bar{z}^3 \tag{35a}$$

$$= 1 + \bar{z}\left(1 + \frac{2}{5}\bar{z}\left(1 + \frac{4}{27}\bar{z}\right)\right), \tag{35b}$$

12

Number of Stages

	1	2	3	4	5	6
α_1	1	0.3333	0.1481	0.0833	0.0533	0.0370
α_2		1	0.4000	0.2069	0.1263	0.0851
α_3			1	0.4265	0.2375	0.1521
α_4				1	0.4414	0.2562
α_5					1	0.4512
α_6						1

Table 1: Multi-stage Coefficients for Optimal First-Order Scheme

Number of Stages

	2	3	4	5	6
α_1	0.4242	0.1918	0.1084	0.0695	0.0482
α_2	1	0.4929	0.2602	0.1602	0.1085
α_3		1	0.5052	0.2898	0.1885
α_4			1	0.5060	0.3050
α_5				1	0.5063
α_6					1

Table 2: Multi-stage Coefficients for Optimal Second-Order ($\kappa = -1$) Scheme

Number of Stages

	2	3	4	5	6
α_1	0.6612	0.2884	0.1666	0.1067	0.0742
α_2	1	0.5010	0.3027	0.1979	0.1393
α_3		1	0.5275	0.3232	0.2198
α_4			1	0.5201	0.3302
α_5				1	0.5181
α_6					1

Table 3: Multi-stage Coefficients for Optimal Third-Order ($\kappa = 1/3$) Scheme

with $\bar{z} = (3/2)z$. The scheme is completely defined by specifying

$$\alpha_1 = \frac{4}{27}, \tag{36a}$$

$$\alpha_2 = \frac{2}{5}, \tag{36b}$$

$$\alpha_3 = 1, \tag{36c}$$

$$\nu = \frac{3}{2}. \tag{36d}$$

As mentioned before, the CFL number achieved in an m-stage scheme optimized for a particular spatial-differencing operator is considerably lower than the maximum CFL number that can be realized using any m-stage scheme. For the first-order upwind-differencing operator, for instance, the maximum CFL number attainable in m steps equals m; in the scheme with optimized high-frequency damping the CFL number amounts to $m/2$. The minimax values of $|P|$ in the high-frequency range are shown in Table 4; the CFL numbers to achieve these are shown in Table 5.

4 Application to a Nonlinear Scalar Equation

A nonlinear convection equation with a source term,

$$\frac{\partial u}{\partial t} + \frac{\partial}{\partial x}\left(\frac{u^2}{2}\right) = \frac{1}{\pi}\sin(\pi x), \qquad x \in [0,1], \tag{37}$$

was chosen for a scalar test of the optimally smoothing multi-stage schemes. The spatial operator was approximated by third-order upwind-biased differencing, corresponding to

14

Number of Stages

Scheme		1	2	3	4	5	6
	First Order	0.7071	0.3333	0.1415	0.0589	0.0244	0.0101
	$\kappa = \frac{2}{3}$		0.8093	0.6521	0.4309	0.3030	0.2073
	$\kappa = \frac{1}{3}$		0.7016	0.4668	0.2950	0.1848	0.1153
	$\kappa = 0$		0.6636	0.4213	0.2579	0.1558	0.0940
	$\kappa = -\frac{1}{3}$		0.6432	0.4009	0.2413	0.1435	0.0851
	$\kappa = -\frac{2}{3}$		0.6289	0.3887	0.2316	0.1364	0.0794
	$\kappa = -1$		0.6179	0.3801	0.2244	0.1315	0.0759

Table 4: $|P|_{max}$ for $\beta \in [\pi/2, \pi]$ for Optimal Schemes

Number of Stages

Scheme		1	2	3	4	5	6
	First Order	0.5000	1.0000	1.5000	2.0000	2.5000	3.0000
	$\kappa = \frac{2}{3}$		0.9132	2.0333	2.3252	3.0438	3.5865
	$\kappa = \frac{1}{3}$		0.8276	1.3254	1.7320	2.1668	2.5975
	$\kappa = 0$		0.7031	1.0560	1.3994	1.7487	2.0976
	$\kappa = -\frac{1}{3}$		0.6055	0.8950	1.1885	1.4844	1.7802
	$\kappa = -\frac{2}{3}$		0.5295	0.7808	1.0371	1.2953	1.5536
	$\kappa = -1$		0.4693	0.6936	0.9214	1.1508	1.3805

Table 5: Optimal CFL number for Optimal Schemes

15

Number of Stages

	2	3	4	5	6
α_1	$\frac{1}{2}$	$\frac{1}{3}$	$\frac{1}{4}$	$\frac{1}{5}$	$\frac{1}{6}$
α_2	1	$\frac{1}{2}$	$\frac{1}{3}$	$\frac{1}{4}$	$\frac{1}{5}$
α_3		1	$\frac{1}{2}$	$\frac{1}{3}$	$\frac{1}{4}$
α_4			1	$\frac{1}{2}$	$\frac{1}{3}$
α_5				1	$\frac{1}{2}$
α_6					1

Table 6: Multi-stage Coefficients for Runge-Kutta Schemes

Equation 28 with $\kappa = 1/3$. Steady solutions were sought on a grid of 512 cells. Two different kinds of marching-schemes were tried:

1. Runge-Kutta multi-stage schemes, with use of the maximum stable CFL number;

2. Optimally smoothing multi-stage schemes.

When using the optimally smoothing multi-stage methods, it is crucial to make the CFL number constant over the entire grid, namely, equal to the unique value derived for maximum damping. This amounts to "local time-stepping" at the prescribed CFL number. For the Runge-Kutta schemes, local time-stepping was used at the highest stable CFL numbers. In cells where the convection speed passes through zero, the time-step must be limited (see, e.g. [8]). For both kinds of schemes, a saw-tooth cycle of multi-grid acceleration was used. All solutions were converged to a factor of 10^{-10} reduction in the residual.

The coefficients for the first six Runge-Kutta schemes are shown in Table 6; the results of these schemes with regard to convergence speed are summarized in Table 7. The computational work needed for convergence, expressed in terms of finest-grid residual calculations, is shown for various numbers of stages and grid levels. It is clear that the maximum-time-step strategy does not combine with the multi-grid strategy; the reason is that the Runge-Kutta schemes, like most schemes, are not good smoothers at the maximum stable CFL number.

The results of the optimally smoothing schemes are shown in Table 8. These schemes clearly are a better match for multi-grid acceleration than the Runge-Kutta schemes. Convergence is reached more quickly in all cases investigated, even on a single grid, despite lower CFL numbers. It is interesting to note that the most efficient of the optimally smoothing schemes, for a sufficient number of grid levels, is the simple two-stage scheme, at least for this simple scalar problem. The gain in smoothing and CFL number achieved with a larger number of stages does not overcome the added computational work.

16

Number of Stages

	2	3	4	5	6
1	1352	933	816	835	942
2	921	581	528	645	585
Grid 3	739	373	350	805	641
Levels 4	1452	**315**	570	919	642
5	1585	326	721	969	744
6	2154	378	749	1034	839

Table 7: Work required for convergence in scalar case — Runge-Kutta schemes with maximum stable CFL number. Work is expressed as number of finest-grid residual calculations.

Number of Stages

	2	3	4	5	6
1	716	627	660	655	660
2	384	365	354	360	369
Grid 3	235	221	224	237	252
Levels 4	169	180	165	188	203
5	**144**	198	163	175	186
6	146	201	166	178	178

Table 8: Work required for convergence in scalar case — Optimally smoothing schemes.

5 Application to a System of Equations

The next series of numerical experiments was based on the quasi-one-dimensional Euler equations for flow in a converging-diverging channel. Only the optimally smoothing multistage schemes were tested. The equations were solved in the form

$$\frac{\partial}{\partial t} \begin{pmatrix} \rho A \\ \rho u A \\ \rho E A \end{pmatrix} + \frac{\partial}{\partial x} \begin{pmatrix} \rho u A \\ (\rho u^2 + p) A \\ \rho u (E + p/\rho) A \end{pmatrix} = \begin{pmatrix} 0 \\ p \frac{dA}{dx} \\ 0 \end{pmatrix} \tag{38}$$

where A is the channel area, given by

$$A(x) = 1 + \frac{1}{2} (1 - \cos(\pi x)), \qquad -1 \leq x \leq 1. \tag{39}$$

Two test cases were run, both with an inflow Mach number $M_\infty = 0.3059$:

1. Shockless transonic flow;

2. Transonic flow with a shock in the diverging portion of the channel.

The Mach number distribution for the second case is shown in Figure 12. In all cases, a sawtooth cycle was used for the multi-grid acceleration, with third-order upwind-biased spatial differencing ($\kappa = 1/3$) on the finest grid, and first-order upwind differencing on all coarser grids. In all cases, the parameters associated with the sawtooth cycle (number of solver applications on finest and on coarser grids) were varied in order to obtain convergence in the least amount of work. Each case was run with local time-stepping and characteristic time-stepping (explained below) for comparison.

The choice of upwind-differencing is not coincidental; in fact it is mandatory for the analysis to extend to the system case. If a conventional approximation is used, based on central-differencing and an artificial viscosity with a scalar coefficient, the loci in the complex plane have a different shape for each wave mode. If upwind-differencing is used, the loci differ merely by a scale factor. Characteristic time-stepping, i.e. use of different time steps for the different characteristic equations such as to make all characteristic CFL numbers equal, can then be used to remove these scale factors.

Characteristic time-stepping is equivalent to preconditioning the Euler residual by a local matrix, rather than a scalar, as in local time-stepping. To show this, the quasi-one-dimensional Euler equations are written as

$$\frac{\partial \mathbf{U}}{\partial t} = -\mathbf{A} (\mathbf{U}) \frac{\partial \mathbf{U}}{\partial x} + \mathbf{s} (\mathbf{U}, x) = \mathbf{Res} (\mathbf{U}) ; \tag{40}$$

for the present analysis the conservation form is not required. The nominal matrix-preconditioned version of this equation reads

$$\frac{\partial \mathbf{U}}{\partial t} = \max_x [\rho (\mathbf{A})] |\mathbf{A}|^{-1} \mathbf{Res}, \tag{41}$$

18
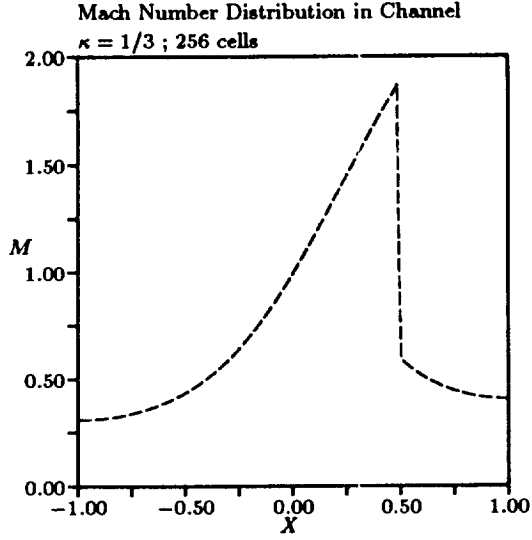
Figure 12: Mach number distribution — Transonic flow with shock

where $\rho(\mathbf{A})$ is the spectral radius of $\mathbf{A}$, and $|\mathbf{A}|$ is the matrix with the same eigenvectors as $\mathbf{A}$ but with the absolute eigenvalues of the latter. In practice each of these eigenvalues may locally vanish, or be very small, making the inversion of $|\mathbf{A}|$ impossible or undesirable. Therefore, Equation 40 will actually be preconditioned according to

$$\frac{\partial \mathbf{U}}{\partial t} = \max_x \left[\rho(\mathbf{A})\right] \left(|\mathbf{A}|^*\right)^{-1} \mathbf{Res}, \tag{42}$$

where the eigenvalues of $|\mathbf{A}|^*$ are bounded away from zero. The lower bound of the eigenvalues of $|\mathbf{A}|^*$ will depend on the magnitude of the local source term. The replacement of the matrix $|\mathbf{A}|$ by a non-singular matrix $|\mathbf{A}|^*$ arises also in the numerical implementation of the so-called entropy condition for first-order hyperbolic system [8].

With only local time-stepping, the preconditioned Euler equations read

$$\frac{\partial \mathbf{U}}{\partial t} = \max_x \left[\rho(\mathbf{A})\right] \left[\rho(\mathbf{A})\right]^{-1} \mathbf{Res}. \tag{43}$$

The work required for convergence of the shockless cases, on a fine grid of 256 cells, is indicated in Tables 9 (local time-stepping) and 10 (characteristic time-stepping). For local time-stepping, one solver on the finest grid and one solver on the coarser grids was most efficient for all cases. For characteristic time-stepping, with six grid levels, it was advantageous to use two or three solver applications on the finest grid. Even then, the performance of the multi-grid relaxation leveled off for more than four grid levels. The reason for this is not yet understood. It is seen that characteristic time-stepping leads to a substantial improvement in convergence speed over local time-stepping. This is to be expected from the analysis, and can be traced to two causes:

1. Characteristic time-stepping removes stiffness due to the variation among characteristic speeds, thus improving the performance of the scheme on a single grid;

Number of Stages

		2	3	4	5	6
	1	6455	5396	5161	4952	4826
	2	1135	1277	1441	1580	1719
Grid	3	822	844	890	938	985
Levels	4	795	783	804	832	875
	5	871	802	800	797	882
	6	632	**589**	625	648	718

Table 9: Work required for convergence — Shockless transonic flow — Local time-stepping

2. By characteristic time-stepping, the optimal CFL number may be used for all waves simultaneously.

The work required for convergence of the cases with a shock is shown in Tables 11 (local time-stepping) and 12 (characteristic time-stepping). For local time-stepping, the strategy of one solver application on each grid was the most efficient, except for a few cases with two or three grid levels. These cases required up to three solver applications on the finest and/or coarser grids. For characteristic time-stepping, the number of solver applications varied from one to eight on the finest grid, and from one to three on the coarser grids. Even with these variations, four of the cases did not achieve a residual drop of 10^{-10}, but got hung up between 10^{-5} and 10^{-9}. Nevertheless, in all converged cases, characteristic time-stepping helped speed up convergence.

Figures 13-15 shed some light on the convergence properties of the schemes tested for the shock case. The comparison between local and characteristic time-stepping can be seen in Figure 13, which shows the two residual histories for the two-stage scheme with five grid levels. The effect of the number of stages on convergence can be seen in Figure 14, which shows the residual histories for characteristic time-stepping and five grid levels. The effect of the number of grid levels can be seen in Figure 15, which shows the residual histories for the two-stage scheme with characteristic time-stepping.

That the multi-grid convergence is basically independent of the number of cells in the finest grid may be seen in Figures 16-19, which show the residual histories for a variety of cases. For each base grid, the numbers of stages and grid levels that gave the best performance were chosen. The convergence histories with characteristic time-stepping (Figures 17 and 19) show the proper behavior, while for local time-stepping, shown in Figures 16 and 18, there is some dependence on the number of cells in the base grid.

Number of Stages

	2	3	4	5	6
1	2432	1968	1881	1808	1760
2	376	449	517	573	632
Grid 3	170	202	235	270	303
Levels 4	**140**	144	157	172	182
5	150	146	159	180	183
6	243	222	218	238	264

Table 10: Work required for convergence — Shockless transonic flow — Characteristic time-stepping

Number of Stages

	2	3	4	5	6
1	11303	9436	9026	8660	8431
2	2608	2846	3152	3438	3695
Grid 3	1719	932	1062	1208	1319
Levels 4	881	817	861	893	946
5	918	826	816	845	890
6	1036	859	844	**807**	845

Table 11: Work required for convergence — Transonic flow with shock — Local time-stepping

Number of Stages

		2	3	4	5	6
	1	6130	5200	5107	—	4584
	2	1589	1608	—	—	—
Grid	3	916	863	987	850	851
Levels	4	639	536	526	587	645
	5	374	365	390	**332**	380
	6	627	429	464	482	579

Table 12: Work required for convergence — Transonic flow with shock — Characteristic time-stepping. Dashes denote cases that did not converge to 10^{-10}.
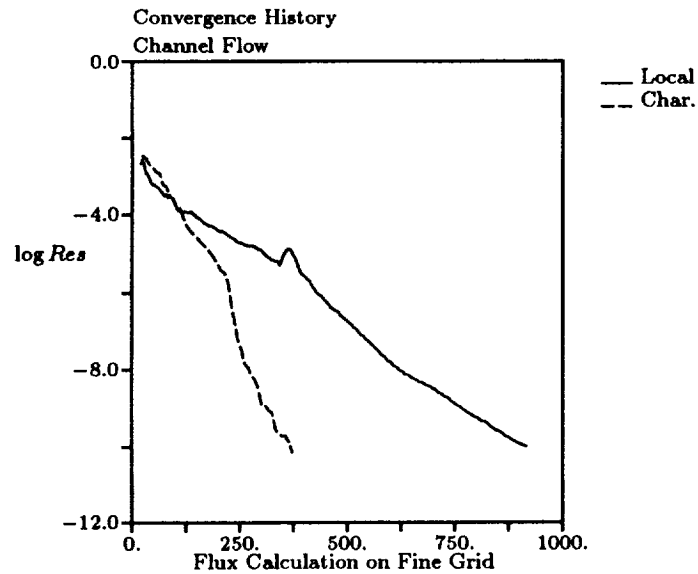

Figure 13: Comparison of local and characteristic time-stepping — Transonic flow with shock — Two stages, five grid levels

22
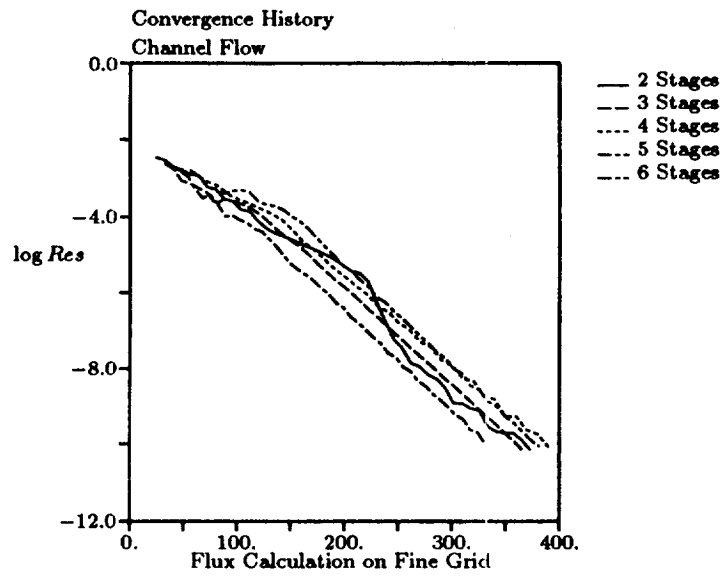
Figure 14: Convergence with different numbers of stages — Transonic flow with shock — Characteristic time-stepping, five grid levels
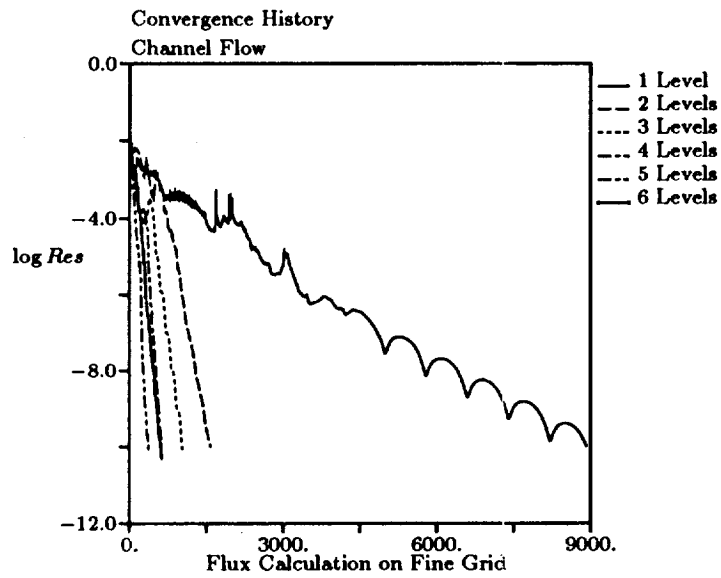
Figure 15: Convergence with different numbers of grid levels — Transonic flow with shock — Characteristic time-stepping, two stages
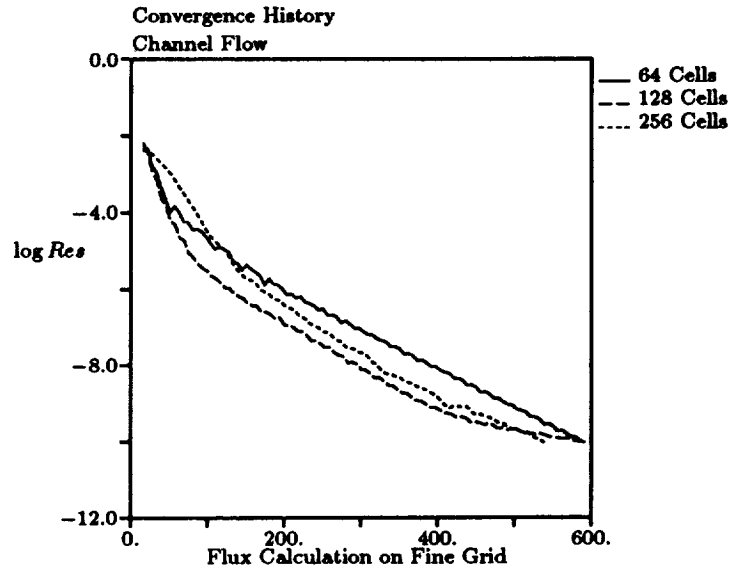
23

Figure 16: Convergence with different base grids — Transonic flow without shock — Local time-stepping, best results per base grid
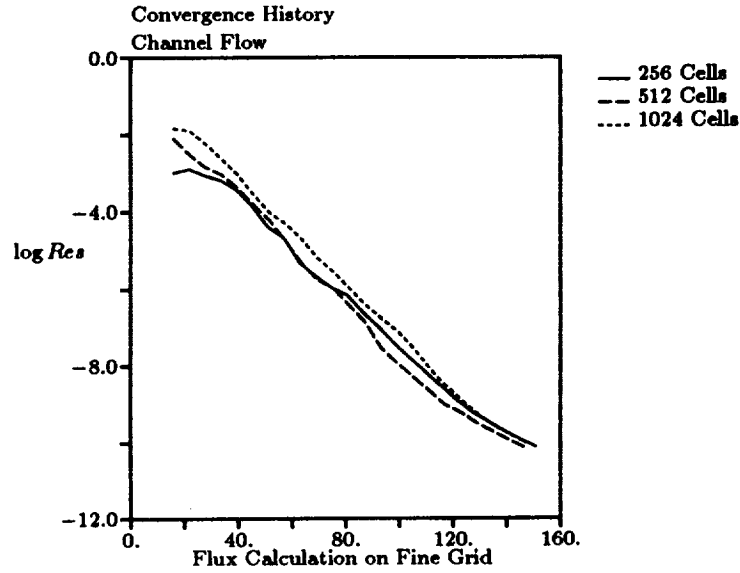

Figure 17: Convergence with different base grids — Transonic flow without shock — Characteristic time-stepping, best results per base grid
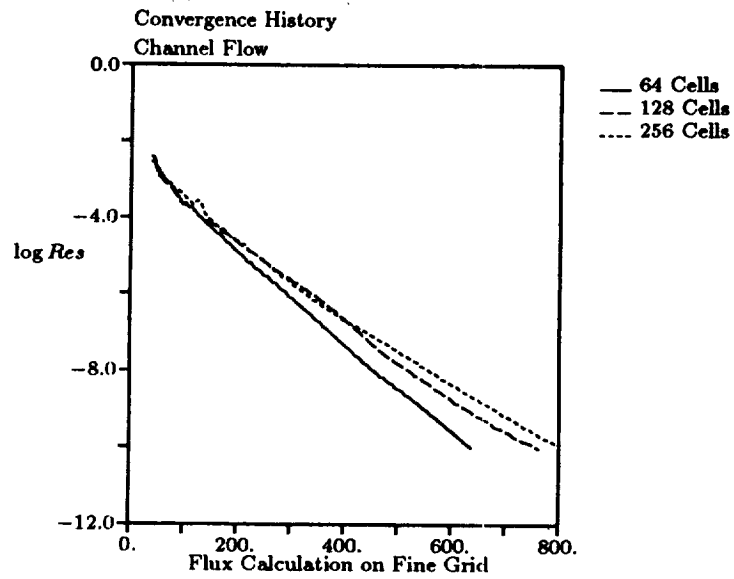
Figure 18: Convergence with different base grids — Transonic flow with shock — Local time-stepping, best results per base grid
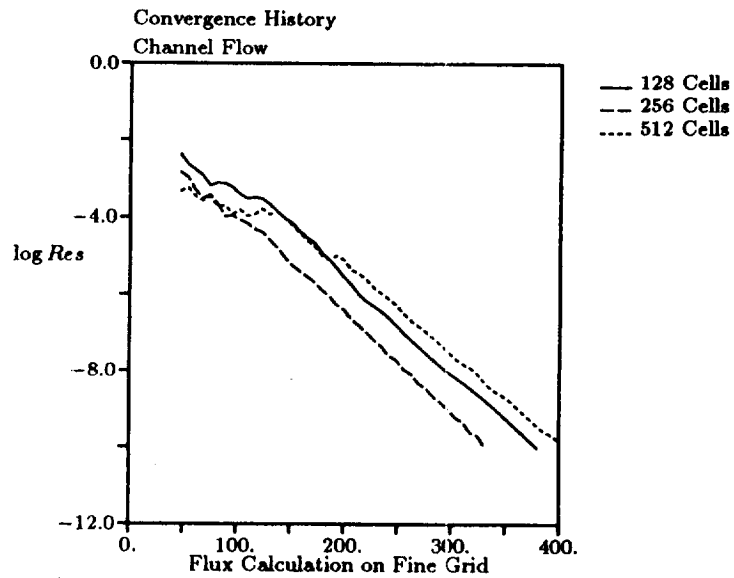

Figure 19: Convergence with different base grids — Transonic flow with shock — Characteristic time-stepping, best results per base grid

6 Application to Multi-Dimensional Equations

A successful extension of the scalar, one-dimensional analysis to the Euler equations in more than one space-dimension stands or falls with the availability of a robust wave-decomposition model. Work on such decompositions is in progress, but has not yet led to reliable schemes. The basis for one possible preconditioning follows.

The two-dimensional Euler equations can be written as

$$\frac{\partial \mathbf{U}}{\partial t} = -\mathbf{A}\left(\mathbf{U}\right)\frac{\partial \mathbf{U}}{\partial x} - \mathbf{B}\left(\mathbf{U}\right)\frac{\partial \mathbf{U}}{\partial y} = \mathbf{Res}\left(\mathbf{U}\right) . \tag{44}$$

There is no obvious way to precondition the residual with a local matrix, as the matrices $\mathbf{A}(\mathbf{U})$ and $\mathbf{B}(\mathbf{U})$ do not have the same eigenvectors, and therefore can not be diagonalized simultaneously. This means Equation 44 can not be written as a system of coupled scalar convection equations. An understanding of the waves that locally pass through the grid can be obtained by assuming some *a priori* knowledge about the types of waves present, and then fitting this model to the local data [9, 10]. The wave model adopted here is based on the Euler equations written in a coordinate system aligned with the local streamline:

$$\frac{\partial \mathbf{U}}{\partial t} = -\mathbf{A}_s\left(\mathbf{U}\right)\frac{\partial \mathbf{U}}{\partial s} - \mathbf{A}_n\left(\mathbf{U}\right)\frac{\partial \mathbf{U}}{\partial n} = \mathbf{Res}\left(\mathbf{U}\right) . \tag{45}$$

The four-component residual vector and, in addition, the two components of the cell-averaged pressure gradient, are then used to obtain the amplitudes of six local waves: two acoustic waves, a shear wave and an entropy wave, all moving along the streamline, and two acoustic waves moving normal to the streamline. Mathematically this means that the residual is rewritten as

$$\mathbf{Res}\left(\mathbf{U}\right) = \mathbf{R}\mathbf{\Lambda}\boldsymbol{\alpha} , \tag{46}$$

where $\boldsymbol{\alpha}$ is the vector of wave strengths, $\mathbf{\Lambda}$ is a 6×6 diagonal matrix carrying the wave speeds in its main diagonal, and $\mathbf{R}$ is a 4×6 matrix built from four eigenvectors of $\mathbf{A}_s$ and two of $\mathbf{A}_n$. The preconditioned equation may now formally be written as

$$\frac{\partial \mathbf{U}}{\partial t} = \mathbf{R}\rho\left(\mathbf{\Lambda}\right)\mathbf{\Lambda}^{-1}\mathbf{L}\,\mathbf{Res}\left(\mathbf{U}\right) \tag{47}$$

$$= \mathbf{M}\;\mathbf{Res}\left(\mathbf{U}\right). \tag{48}$$

The 6×4 matrix $\mathbf{L}$ is a generalized inverse of $\mathbf{R}$ and therefore not uniquely defined. Research is presently focusing on finding an inverse, using physical or mathematical arguments, that makes the preconditioning by $\mathbf{M}$ truly effective.

It should be noted that, even if a suitable preconditioning matrix M is developed, the optimally-smoothing schemes are "tuned" to filter waves travelling in the propagation direction (c_x, c_y) of the problem being solved. For optimal performance in two dimensions, something must be done about high-frequency waves normal to this direction. For a convection problem defined by

$$c_x\frac{\partial}{\partial x} + c_y\frac{\partial}{\partial y} , \tag{49}$$

26

Stages

	2	6
1	8821	7404
2	2455	3145
3	2458	1758
4	2380	**1684**

Grid Levels

Table 13: Work required for convergence — Two-dimensional case — Local time-stepping

a derivative in the direction normal to the propagation direction is given by

$$c_y \frac{\partial}{\partial x} - c_x \frac{\partial}{\partial y} \, , \qquad (50)$$

and a positive-definite operator which acts in this normal direction is given by

$$c_x^2 \frac{\partial^2 u}{\partial^2 y} - 2c_x c_y \frac{\partial^2 u}{\partial x \partial y} + c_y^2 \frac{\partial^2 u}{\partial x^2} \, . \qquad (51)$$

Unfortunately, adding this term would reduce any scheme to first order. Methods of adding this term in a non-linear manner are being studied, to give optimal damping without reducing the order of the solution in the steady state.

Since the work on the preconditioning matrix and the cross-diffusion terms mentioned above is still in progress, the two-dimensional Euler equation results presented here are for local time-stepping with no cross-diffusion. The test case was a NACA 0012 airfoil at zero incidence in a $M_\infty = 1.2$ freestream. This case has a bow shock and a fishtail shock. First-order upwind-differencing was used. Table 13 summarizes the number of finest-grid residual calculations necessary for convergence (to 10^{-10}) on a 64 × 32 grid. In the six-stage, four grid-level scheme, three iterations on the finest grid followed by one on each of the coarser grids were used; for all other schemes, one iteration on each grid was used. Despite the use of local time-stepping as a substitute for characteristic time-stepping, the multi-stage schemes combined well with the multigrid acceleration.

7 Conclusions and Future Research Directions

In these notes, a method has been developed for designing optimally smoothing multi-stage time-marching schemes, given any spatial-differencing operator. Such schemes are particularly useful in conjunction with multi-grid acceleration. The advantage of using these optimally smoothing schemes has been demonstrated by comparison with Runge-Kutta schemes in solving a nonlinear scalar equation. The analysis has been extended to the Euler equations

in one space-dimension by use of characteristic time-stepping. Convergence rates independent of the number of cells in the finest grid have been achieved with these optimal schemes, for transonic flow with and without a shock. Besides characteristic time-stepping, local time-stepping has been tested with these schemes. While the analysis is only truly applicable with characteristic time-stepping, good convergence has still been obtained with local time-stepping. The extension to two-dimensional flows is hampered by the lack of a robust two-dimensional wave model that may serve as the basis of characteristic time-stepping, and by the lack of a method to damp high-frequency waves normal to the direction of propagation. Future research must concentrate on these two issues. Only with these techniques may full advantage be taken of the optimally smoothing multi-stage schemes.

Acknowledgments

References

[1] R. M. Beam and R. F. Warming, "An implicit finite-difference algorithm for hyperbolic systems in conservation law form," *Journal of Computational Physics*, vol. 22, 1976.

[2] K. G. Powell, "Computation of compressible vortical flows," in *Computational Fluid Dynamics*, Von Kármán Institute for Fluid Dynamics, Lecture Series 1990-04, 1990.

[3] A. Jameson, W. Schmidt, and E. Turkel, "Numerical solutions of the Euler equations by a finite-volume method using Runge-Kutta time-stepping schemes," AIAA Paper 81-1259, 1981.

[4] A. Brandt, "Multilevel adaptive computations in fluid dynamics," *AIAA Journal*, vol. 18, 1980.

[5] A. Jameson, "Numerical solution of the Euler equations for compressible inviscid fluids," in *Numerical Methods for the Euler Equations of Fluid Dynamics* (F. Angrand, A. Dervieux, J. A. Désidéri, and R. Glowinski, eds.), SIAM, 1985.

[6] B. van Leer, C. H. Tai, and K. G. Powell, "Design of optimally-smoothing multi-stage schemes for the Euler equations," in *AIAA 9th Computational Fluid Dynamics Conference*, 1989.

[7] B. van Leer, "Upwind-difference methods for aerodynamic problems governed by the Euler equations," in *Large-Scale Computations in Fluid Mechanics, Lectures in Applied Mathematics*, vol. 22, 1985.

[8] B. van Leer, W. T. Lee, and K. G. Powell, "Sonic-point capturing," in *AIAA 9th Computational Fluid Dynamics Conference*, 1989.

[9] P. L. Roe, "Discrete models for the numerical analysis of time-dependent multidimensional gas-dynasmics," *Journal of Computational Physics*, vol. 63, 1986.

[10] K. G. Powell, B. van Leer, and P. L. Roe, "Towards a geunuinely multi-dimensional upwind scheme," in *Computational Fluid Dynamics*, Von Kármán Institute for Fluid Dynamics, Lecture Series 1990-04, 1990.